

Article

Adhesion Strength of Al, Cr, In, Mo, and W Metal Coatings Deposited on a Silicon–Carbon Film

Natalia Igorevna Cherkashina *, Vyacheslav Ivanovich Pavlenko, Sergey Viktorovich Zaitsev ,
Andrey Ivanovich Gorodov, Semen Nikolayevich Domarev, Roman Vladimirovich Sidelnikov
and Dmitry Sergeevich Romanyuk

Department of Theoretical and Applied Chemistry, Belgorod State Technological University Named after V.G. Shukhov, 308012 Belgorod, Russia; belpavlenko@mail.ru (V.I.P.); sergey-za@mail.ru (S.V.Z.); gorodov-andrey@mail.ru (A.I.G.); domarev542@gmail.com (S.N.D.); roman.sidelnikov@mail.ru (R.V.S.); romanyuk.dmitrij.98@bk.ru (D.S.R.)

* Correspondence: cherkashina.ni@bstu.ru

Abstract: For the first time, the possibility of creating a multilayer system metal (Al, Cr, In, Mo, and W) silicon–carbon coating was studied. A silicon–carbon film was synthesized from a polyorganosiloxane polymer containing an active Si–O siloxane group. Due to the use of furnace pyrolysis, in which the purge gas continuously removes the polymer thermal degradation products from the system, it was possible to reduce the film formation temperature to 300 °C. According to the energy dispersive analysis data, silicon–carbon film has the following composition: C—34.85 wt%, O—42.02 wt%, and Si—23.13 wt%. Metallic coatings of Al, Cr, In, Mo, and W on a silicon–carbon substrate were obtained by vacuum magnetron sputtering. The metallic coatings were evaluated by SEM as well as by X-ray phase analysis. The adhesion strength of metallic coatings to the silicon–carbon substrate was assessed by scratching under continuously increasing load with a Rockwell C Diamond Indenter. At the same time, the friction coefficient was recorded at the corresponding value of load on the indenter. The adhesive strength of metals with the silicon–carbon substrate increases in the sequence W, Mo, In, Al, and Cr.



Citation: Cherkashina, N.I.; Pavlenko, V.I.; Zaitsev, S.V.; Gorodov, A.I.; Domarev, S.N.; Sidelnikov, R.V.; Romanyuk, D.S. Adhesion Strength of Al, Cr, In, Mo, and W Metal Coatings Deposited on a Silicon–Carbon Film. *Coatings* **2023**, *13*, 1353. <https://doi.org/10.3390/coatings13081353>

Academic Editor: Braham Prakash

Received: 23 June 2023

Revised: 14 July 2023

Accepted: 27 July 2023

Published: 2 August 2023



Copyright: © 2023 by the authors. Licensee MDPI, Basel, Switzerland. This article is an open access article distributed under the terms and conditions of the Creative Commons Attribution (CC BY) license (<https://creativecommons.org/licenses/by/4.0/>).

Keywords: polyorganosiloxane polymer; metal coatings; magnetron sputtering method; adhesion strength; friction coefficient

1. Introduction

Semiconductor materials are widely used to make semiconductor diodes, transistors, and integrated circuits. Semiconductors are essential to the operation of all electronic equipment, from home computers to unmanned car circuits. The most widely used conductors are based on silicon and gallium arsenide, which have optical properties [1,2]. They are used in the production of solar panels and LEDs.

Despite the high popularity and efficiency of silicon semiconductors, scientists from all over the world are currently working to develop new technologies to produce high-efficiency semiconductors [3,4]. There are two factors that are pushing manufacturers to accomplish this. Firstly, the technology has almost reached its limits, beyond which it will be impossible to create ever-smaller and more powerful devices. Secondly, the constant growth in demand for silicon leads to a significant increase in its price. The materials based on silicon oxide and silicon carbide, as well as silicon oxycarbide, are of particular interest. Despite the widespread availability of silicon oxide in nature, it is necessary to use a particularly pure oxide without impurities in order to apply it as a semiconductor. In addition, the phase structure of SiO₂ is particularly important. For example, high annealing or hydrothermal treatment is required to convert it from amorphous to crystalline state [5–8].

Silicon oxycarbide is a superposition of amorphous silica (SiO_2) and silicon carbide (SiC) [9]. It has good physical and mechanical characteristics and thermal and chemical stability [10–12]. It is known that silicon oxycarbide can be obtained using pyrolysis of organosilicon polymer precursors [13]. Despite many works on the research and application of silicon oxycarbide, the creation of a system of a metal–silicon oxycarbide semiconductor has not been considered so far. Consideration of contacts between metal and a silicon oxycarbide semiconductor is of interest because they find application as rectifier contacts in Schottky diodes, as well as in non-rectifier, or ohmic, contacts for input and output voltages and currents in insulating junctions and semiconductor devices [14,15].

The future of electronics is associated with the development of such layered materials. First of all, this will allow changing the physical dimensions of microcircuit elements and creating nanotransistors. It is calculated that the nanotransistor will run faster and consume less power [16].

The application of metal coatings can be carried out by several methods. The main methods of thin-film deposition are vacuum evaporation (sputtering) with indirect heating; ion–plasma sputtering; deposition from the gas phase using gas-transport reactions; reduction in a hydrogen atmosphere, and thermochemical decomposition, etc. [17–19]. The choice of one or another method depends on the nature of the deposited material, substrate material, structure (amorphous, polycrystalline, or monocrystalline), and the thickness of the metal film [20–23]. In [24], the method of obtaining metallic layers on semiconductors by the electrochemical method is presented. The electrochemical method of metal deposition is quite simple, technological, easily controllable, and low-temperature, which makes it preferable for wide production. The authors studied the processes of chemical deposition of Ag, Co, Cu, Zn, Sn, and Ni on *p*-Si from water solutions. Another work [25] shows the method of deposition of aluminum thin films on SiO_2/Si substrates by magnetron sputtering. It was found that increased sputtering power enhances the crystallinity of the deposited Al films. In [26], it was possible to create a film of metallic Ag on an amorphous and crystalline α -quartz SiO_2 substrate by thermal decomposition of Ag oxalate at approximately 200 °C.

When making a metal film, special attention is paid to the adhesion properties. The adhesion strength of Pt, Cu, and Ti metals with Si and SiO_2 surfaces with different roughness was investigated in [27]. It was found that changes in the chemical composition of the surface had a greater effect than roughness on the adhesive strength of the systems studied.

This paper presents the results of the research on the adhesion strength of Al, Cr, In, Mo, and W metallic coatings on a silicon–carbon film substrate obtained by pyrolysis of an organosilicon liquid.

2. Materials and Methods

2.1. Silicon–Carbon Film Synthesis

Polyalkylhydrosiloxane liquid containing the active siloxane group Si–O (Point LLC, St. Petersburg, Russia) was used for the synthesis of the silicon–carbon film. Chemically pure n-hexane (JSC ECOS-1, Moscow, Russia) was used as a solvent in the amount of 70 wt.%. Silicon–carbon film was formed on 1 mm thick glass slides.

The formation of the silicon–carbon film on the glass slides was carried out in glass beakers with a lid at a total volume of the reaction mixture of 49.4 mL for each unit of glassware. The glass slides were kept in the solution for 15 min. After that, the slides were removed and heat-treated in the drying oven. The initial temperature was 60 °C, with an exposure time of 90 min. Then, the temperature was gradually raised to 300 °C. At 100 °C, the film was incubated for 30 min, and then the temperature was raised to 150 °C and the film was incubated for another 30 min at 200 °C, where it was kept for 30 min; at 250 °C, it was incubated for another 30 min, and, finally, the film was exposed to the maximum temperature of 300 °C also for another 30 min. After that, the substrate with the film was cooled to room temperature. Gradual rise in temperature is due to the fact that, with increasing temperature, the number of formed particles grows and the reaction

proceeds faster, so the silicon–carbon film is evenly fixed on the glass slide by means of a gradual increase in temperature.

2.2. Metallic Coating Application

The metallic coatings Al, Cr, In, Mo, and W were applied to the substrates with a silicon–carbon film using dual magnetron sputtering in the UniCoad 200 vacuum machine with an unbalanced magnetic system. Before sputtering the coatings, the substrates were washed with ethanol and dried in a stream of dry nitrogen. The vacuum chamber was evacuated to the pressure of $9 \cdot 10^{-3}$ Pa, which was achieved using a diffusion (steam–oil) pump. The pumping rate was 790 L/min at a pressure of 0.005 Pa. To remove residual contaminants, the surface of the substrates was cleaned with argon ions. The ion cleaning was performed for 8 min at the pressure of $8 \cdot 10^{-2}$ Pa and the voltage of the ion source of 1.8 kV. The coatings were deposited from two vertically mounted targets (cathode) by sputtering the corresponding metal in the Ar atmosphere at the pressure of 0.17 ± 0.01 Pa. The rotation speed of the samples was 20 rpm to achieve uniform deposition. The distance from the substrates to the magnetron and ion source was 70 mm. During coating, the substrate was not additionally heated. Table 1 shows the conditions of applying metallic coatings of Al, Cr, In, Mo, and W.

Table 1. Technological conditions of the metal coating process.

Coating	Parameters			
	Magnetron Discharge Current, A	Discharge Voltage, V	Frequency, kHz	Displacement Voltage Us, V
Al	2	447/435 *	18	20
Cr	2	461/451		
In	1	453/449		
Mo	2	420/416		
W	1	405/397		

* the values for each magnetron are provided.

The parameters indicated in Table 1 were determined experimentally for each metal coating. With these parameters, there is no overheating of the silicon–carbon film substrate. The maximum temperature at the specified parameters did not exceed 200 °C. Since the thickness of the silicon–carbon film is small, at a higher temperature, it could be deformed and warped. Also, with the indicated parameters, stable electrophysical characteristics of metal coatings were obtained. With the parameters indicated in Table 1, the metal coatings behaved like a massive electrical conductor; i.e., specific electrical resistance was equal to the resistance of pure metal.

2.3. Research Methods

Scanning electron microscope MIRA3 TESCAN (Tescan, Brno, Czech Republic) was used to study the surface morphology and thickness of the coatings.

The crystalline structure of the coatings was studied using X-ray diffraction (ARL X'TRA, Thermo Fisher Scientific, Waltham, MA, USA) with CuK α source in the range of 2 θ angles from 4° to 70° in the asymmetric coplanar shooting mode with a sliding incidence angle $\alpha = 3^\circ$ (θ -scan). Phase identification and peak indexing were performed using the ICDD (International Centre for Diffraction Data) JCPDF database JCPDF database.

Adhesion strength of the coatings was evaluated on the MFT-2000A scratch tester (Rtec Instruments, Oakland, CA, USA) using a Rockwell cone indenter with an apex angle of 120° and a tip rounding radius of 200 μ m. At the end of each test, the scratch trace of the coatings was evaluated using the SIAMS 800 solid microstructure fragment analyzer (SIAMS LLC, Yekaterinburg, Russia).

3. Results and Discussion

3.1. Study of Silicon–Carbon Film

Figure 1 shows a scheme of thermal degradation of polyorganosiloxane polymer, on the basis of which a silicon–carbon film of $\text{Si}_x\text{C}_y\text{O}_z$ composition can be obtained as a result of temperature treatment at $\sim 300^\circ\text{C}$. The Si/C ratio can be controlled by choosing the organic substituents (R_1 and R_2) at the silicon atom.

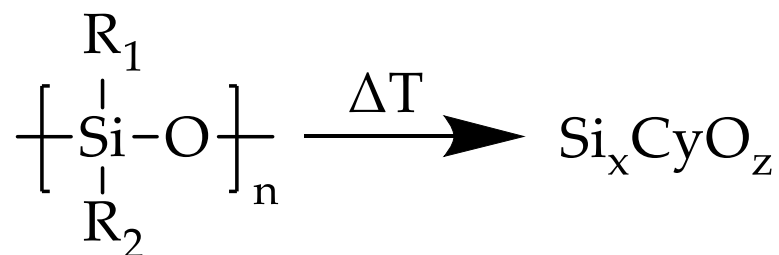


Figure 1. Scheme of thermal degradation of polyorganosiloxane polymer.

After formation and solidification (intermolecular cross-linking) of polyorganosiloxane polymer on the slide glass, a film is formed as a result of destruction and removal of organic groups (methyl, phenyl, and vinyl), as well as Si–H- and Si–OH- groups [28]. Such processes usually proceed at high temperatures ($\sim 1000^\circ\text{C}$). In this study, we used furnace pyrolysis, in which the purge gas continuously removes polymer thermal degradation products from the system [29]. This reduced the firing temperature to 300°C .

Figure 2 shows the SEM image data of the film obtained from the polyalkylhydrosiloxane liquid.

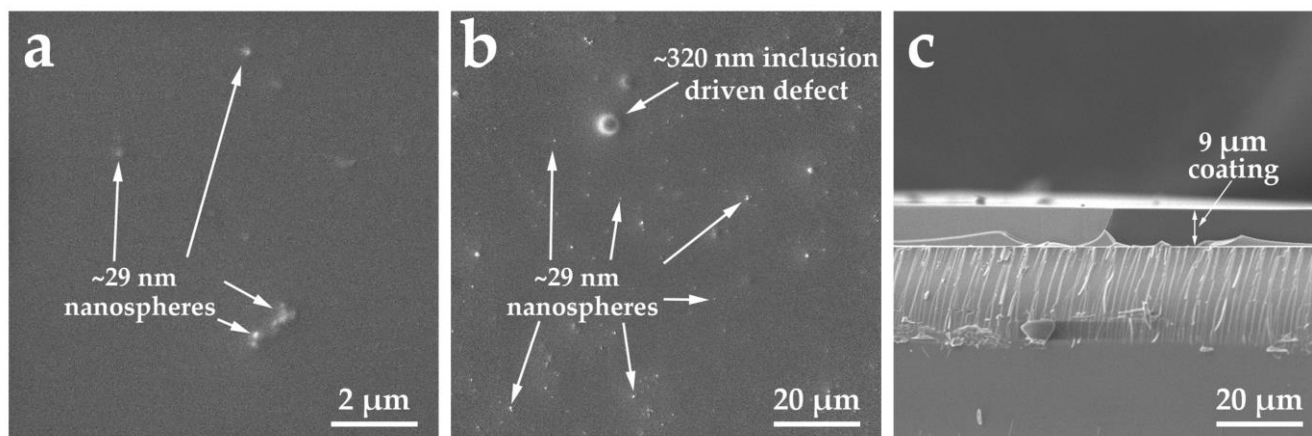


Figure 2. SEM image of the film obtained from the polyalkylhydrosiloxane liquid: (a,b) surface morphology; (c) cross-sectional chipping of the film.

The analysis of the data in Figure 2 showed that the film obtained from the polyalkylhydrosiloxane liquid is quite homogeneous, without delaminations and chips. On the surface of the film, one can notice a number of nanospheres with a diameter of 29 nm. The analysis of the cross-sectional chipping (Figure 2c) showed that the film thickness was almost the same along the entire length of its contact with the substrate and was $\sim 9\ \mu\text{m}$. In Figure 2c, the boundary between the film and the substrate is clearly visible. It can also be noted that the film was formed quite tightly on the glass slide: no detachment of the film from the substrate was detected.

The elemental composition of the film was determined by X-ray spectral analysis. The composition was determined by averaging the experimental data by three measurements in

different points of the sample. Experimental data on determining the chemical composition of the film are presented in Table 2.

Table 2. Elemental composition of polyalkylhydrosiloxane film.

C, at. %	O, at. %	Si, at. %
34.85	42.02	23.13

As was expected, the film has the $\text{Si}_x\text{C}_y\text{O}_z$ composition and can be called a silicon–carbon film. No atoms of other elements were recorded. The experiments showed that all Si, C, and O atoms are distributed almost homogeneously along the film depth.

The structure of the silicon–carbon film was studied by the method of X-ray phase analysis. Figure 3 shows the X-ray diffraction pattern of the silicon–carbon film. It was found that the structure of the film was completely amorphous. There are two pronounced amorphous halos at angles $2\theta = 9^\circ$ and 23° on the X-ray diffraction pattern.

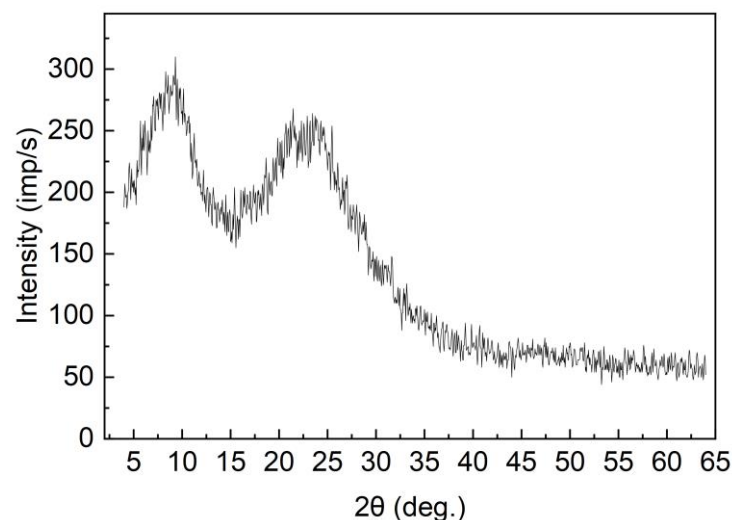


Figure 3. X-ray diffraction pattern of the silicon–carbon film.

3.2. Study of Al, Cr, In, Mo, and W Metal Coatings

Figure 4 shows the X-ray diffraction patterns of the obtained metallic coatings using the method of vacuum magnetron sputtering of the corresponding targets. The use of the sliding beam technique to obtain the X-ray diffraction patterns made it possible to register the characteristic radiation of the atoms of the crystal lattice only of the Al, Cr, In, Mo, and W metal coatings and exclude the appearance of reflexes corresponding to the lattice of the silicon–carbon substrate. This became possible because the X-ray penetration depth at a very small angle is much less than the thickness of the Al, Cr, In, Mo, and W metal coatings.

The X-ray diffraction pattern of the coating obtained by sputtering of the Al target (Figure 4a) is typical for crystalline aluminum diffraction reflexes in regions (111), (200), and (211). The presence of X-ray maximums of different orders of reflection from crystallographic planes is consistent with the International X-ray Database PDF-2 (Al card No. 85-1327). The presence of narrow high diffraction peaks on the Al X-ray diffraction pattern indicates that the coating is well-oxidized and homogeneous in lattice parameters. The resulting thin aluminum coating has a polycrystalline structure with a face-centered cubic lattice. The intensity of the reflexes of the aluminum coating reflected by the plane (111) significantly exceeds the intensities of the other peaks, which suggests a high degree of structuring of the crystal lattice.

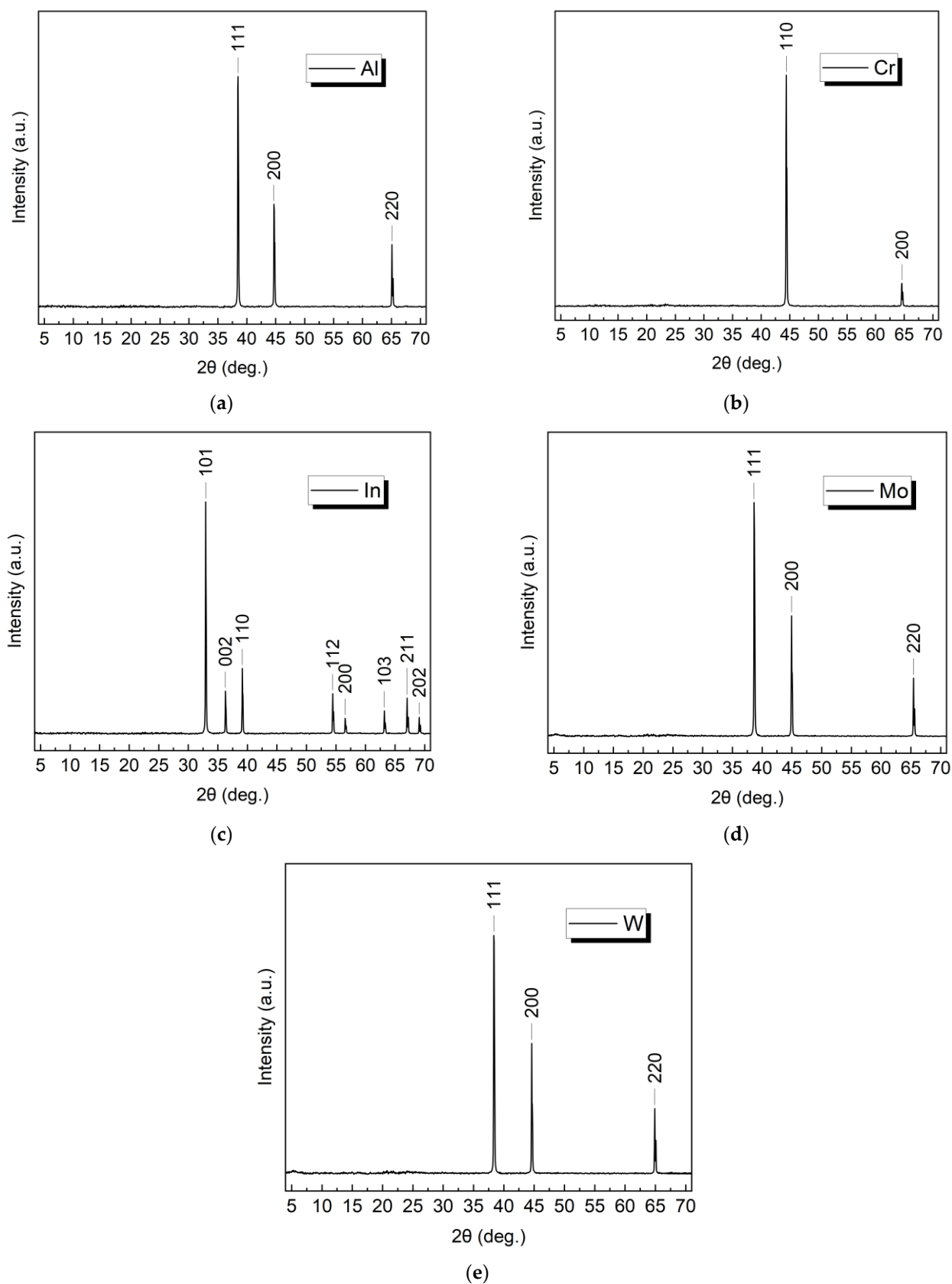


Figure 4. X-ray diffraction patterns of metal coatings obtained using the method of vacuum magnetron sputtering of the corresponding targets: (a) Al; (b) Cr; (c) In; (d) Mo; (e) W.

The X-ray diffraction pattern of the coating obtained by sputtering of the Cr target (Figure 4b) corresponds to the X-ray pattern of metallic Cr according to the X-ray Database PDF-2 (card Cr No. 85-1335). Three diffraction peaks corresponding to (110), (200), and (211) crystal planes of a volume-centered cubic lattice were recorded on the X-ray diffraction pattern.

The X-ray diffraction pattern of the coating obtained by sputtering of the In target (Figure 4c) shows the following diffraction reflexes in regions (002), (101), (103), (110), (112), (200), (202), and (211). The resulting X-ray diffraction is fully consistent with metallic indium (card In No. 85-1409). The obtained indium coating also has a polycrystalline structure, but with a tetragonal face-centered lattice.

As can be seen from Figure 4d, the X-ray diffraction pattern of the coating obtained by sputtering of the Mo target contains the reflexes reflected by crystallographic planes (111), (200), and (220). As the results of X-ray diffraction analysis show, the coating corresponds to the Mo card No. 88-2331. The obtained molybdenum coating is well-oxidized and has a polycrystalline structure with a volume-centered cubic lattice.

According to Figure 4e, it was found that the diffractogram of the coating obtained by sputtering of the W target was metallic tungsten (PDF card No. 4-806); no additional peaks were detected. Reflexes reflected by crystallographic planes (110) and (200) were recorded on the X-ray diffraction. Tungsten crystals have a volume-centered cubic lattice.

Figure 5 shows SEM images of the surface of the obtained metallic coatings, as well as their cross-sectional chips.

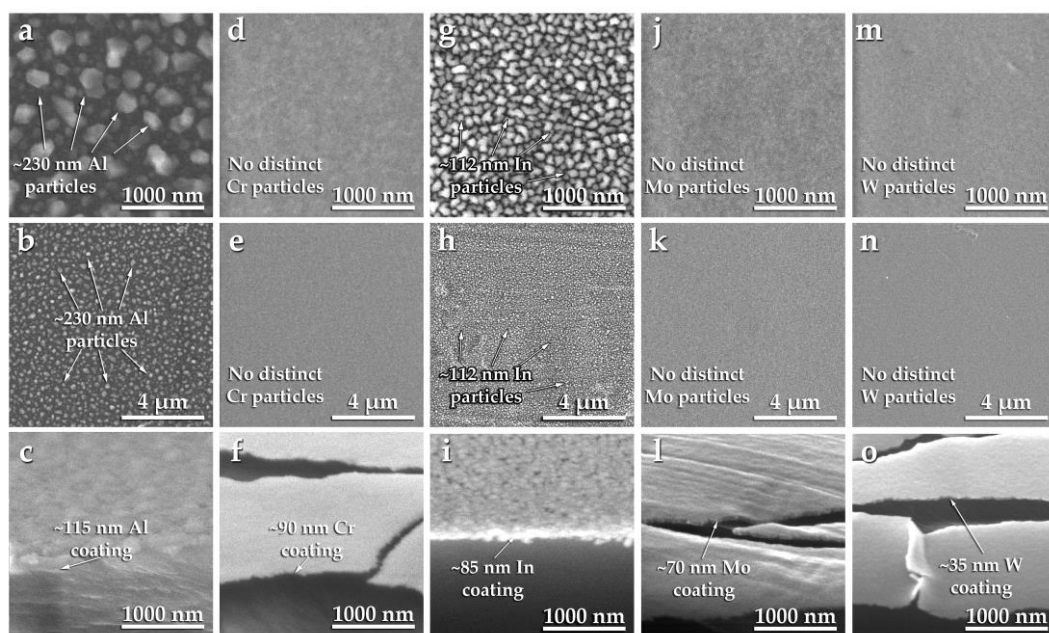


Figure 5. SEM images of the surface of the obtained metallic coatings: (a,b) Al; (d,e) Cr; (g,h) In; (j,k) Mo; (m,n) W, as well as their cross-sectional chips: (c) Al; (f) Cr; (i) In; (l) Mo; (o) W.

The structure of the Al coating is a granular (spongy) surface. The electron microscopy results (Figure 5a,b) show that the Al crystallites have a dispersed, homogeneous nanostructure. The SEM image of the cross-sectional chip (Figure 5c) clearly shows a defect-free transition region between the silicon–carbon substrate and the aluminum coating. The thickness of the applied metallic aluminum coating is almost the same along the entire length of the chip surface and is ~115 nm.

The surfaces of Cr, Mo, and W metal coatings are fairly uniform and smooth (Figure 5). Meanwhile, when sputtering the In target, the coating has a rougher surface morphology. Individual spherical crystallites of In can be observed here. The morphology of the In metal coating is characterized by a porous and heterogeneous structure with a coating thickness

of ~85 nm. This is due to the fact that bombardment with In ions can cause sputtering and formation of structural defects, which are the sources of microstructure heterogeneity. With a thicker coating, the structure will be more homogeneous and the concentration of defects will be greatly reduced. As the coating is deposited, the surface heats up where it condenses. This causes increased diffusion of atoms, which can result in a more perfect microstructure.

All the metallic coating samples (Al, Cr, In, Mo, and W) have a microstructure close to a columnar one, which corresponds to the classical model concepts of the coating structure [30]. The Cr coating thickness is 90 nm, Mo coating thickness is 70 nm, and W coating thickness is 35 nm. The interface between the applied Al, Cr, In, Mo, and W metallic coatings and the silicon–carbon substrate can be traced over the entire survey area.

3.3. Adhesive Properties

To determine the adhesion strength of Al, Cr, In, Mo, and W metal coatings to a silicon–carbon substrate, the samples under study were scratched under continuously increasing load using a Rockwell C Diamond Indenter with a tip radius of 200 μm . The friction coefficient was recorded at the corresponding value of load on the indenter. In order to obtain reliable results, three scratches were applied to the surface of the coated samples on each sample. The tests were performed under the following conditions: the load on the indenter increased from 0.1 to 10 N, the indenter travel speed was—4 mm/min, the scratch length was 4 mm, and the loading speed was 9.9 N/min. All tests were performed at 23 °C. The moment of adhesive or cohesive fracture of the coating was recorded after the tests by visual inspection using an optical microscope equipped with a digital camera. The tests of the adhesion strength of Al, Cr, In, Mo, and W metal coatings to the silicon–carbon substrate determined

- minimum (critical) load L_{c1} , which denotes the moment when the first crack appears;
- L_{c2} —peeling of coating segments or appearance of multiple cracks;
- L_{c3} —plastic abrasion of the coating up to the substrate.

Figure 6 shows curves of the friction coefficient dependence on the indenter load obtained when studying the adhesion strength of all Al, Cr, In, Mo, and W metal coatings on a silicon–carbon substrate. The panorama photographs of the scratch grooves obtained by loading the indenter onto the corresponding metal coating are shown in Figure 7. Also, Figure 7 shows the areas corresponding to the critical forces determined on the basis of the optical photographs of the scratch grooves. Figure 7 shows the areas L_{c1} , L_{c2} , and L_{c3} . The load values at which cracks begin to appear (L_{c1}), the value at which multiple cracks appear (L_{c2}), as well as the values of adhesion strength of metal coatings with silicon–carbon substrate (L_{c3}) are presented in Table 3.

Table 3. Values of adhesion properties of metal coatings.

Metal Coating	Critical Loads					
	L_{c1}		L_{c2}		L_{c3}	
	[N]	[J/m ²]	[N]	[J/m ²]	[N]	[J/m ²]
Aluminum	2.78	0.445	4.22	0.796	6.26	0.628
Chromium	1.47	0.118	4.37	0.024	6.51	0.012
Indium	2.06	3.431	4.61	4.259	6.07	2.930
Molybdenum	2.98	0.198	4.48	0.208	6.03	0.128
Tungsten	1.55	0.168	3.64	0.071	4.86	0.019

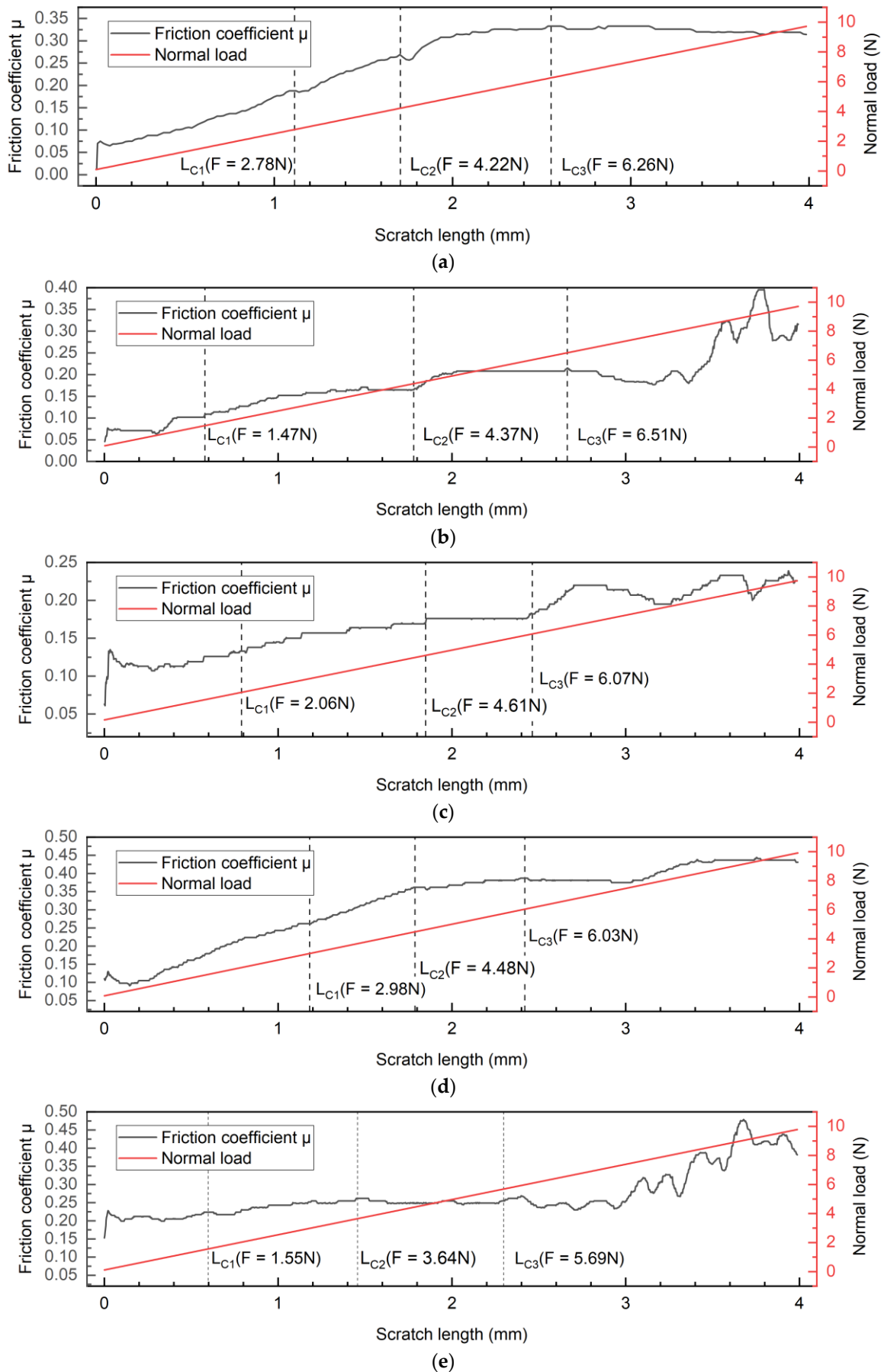


Figure 6. Scratch test diagram registered for coating: (a) Al; (b) Cr; (c) In; (d) Mo; (e) W.

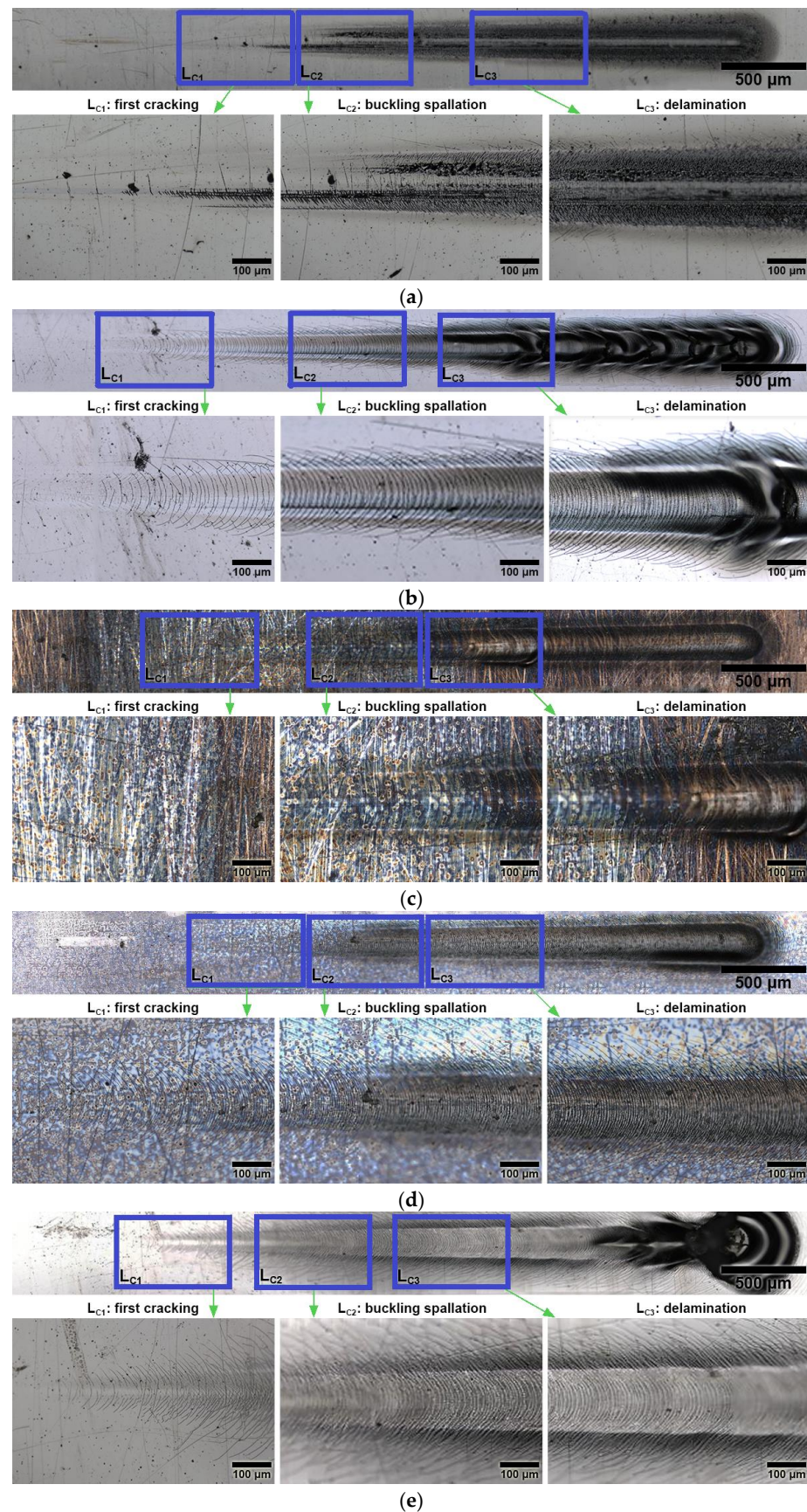


Figure 7. Panorama photograph of the scratch groove on the coating: (a) Al; (b) Cr; (c) In; (d) Mo; (e) W, revealing the connection between the different sub/critical loads and the related damage mechanisms.

The work of adhesion (W , J/m²) at critical load (L_c) was calculated using the formula proposed by Bull et al. [31]:

$$W = \frac{\left(\frac{L_c \cdot \vartheta \cdot \mu}{A_1}\right) \cdot t}{2E}$$

where L_c is the critical load, N; ϑ is Poisson's ratio; μ is the coefficient of friction; A_1 —cross-sectional area of the scratch track at the point where the critical load L_c is reached, m²; t is the coating thickness, m; E is Young's modulus, Pa.

The work of adhesion is different for each critical load as it corresponds to different modes of coating failure (e.g., «first cracking», «buckling spallation», or «delamination»).

The analysis of the photos of the scratches (Figure 7) showed that cracking of the coating on the substrate surface due to indentation is typical for all the studied metals. No significant peeling was detected for all metal types. The comparative analysis of the obtained data on the adhesion strength (Figure 7) shows that the Al, Cr, In, Mo, and W metal coatings on the silicon–carbon substrate abrade under scratching, but they do not peel. It can be claimed that the coatings fail by the cohesive mechanism associated with plastic deformation and formation of fatigue cracks in the coating material. All the metallic coatings are characterized by the fact that, under load L_{c1} , microcracks are initiated on both sides of the indenter passage and spread as the indenter progresses. This is clearly shown in Figure 7. It can also be noted that, when the first cracks and chips appear (L_{c1}), there is an increase in the friction coefficient accompanied by a small jump on the curve (Figure 6). After load L_{c1} , the continuation of crack formation on both sides of the indenter stroke is observed. The value of load L_{c2} corresponds to the areas in which multiple cracks appear on both sides of the scratch (Figure 7). The value of load L_{c3} is taken as the value of adhesion strength of metal coating, at which plastic abrasion of metal coating to silicon–carbon substrate is observed. This failure mode is characteristic of coatings that have low adhesion strength and possess high compressive residual stresses [32].

Despite the similar nature of the adhesive failure of metal coatings on a silicon–carbon substrate, the coatings have different values of adhesion strength. The tungsten coating has the worst adhesion strength (L_{c3}), and the chromium coating has the best one. The first scratches (L_{c1}) appear the fastest on the chromium coating, and the molybdenum coating remains crack-free the longest.

4. Conclusions

For the first time, the possibility of obtaining a silicon–carbon film from a polyorganosiloxane polymer as a result of heat treatment at ~300 °C, as well as the deposition of metal coatings (Al, Cr, In, Mo, and W) on it, was established. According to scanning electron microscopy, the thickness of the silicon–carbon film was determined to be ~9 μm. It has been established that the film thickness is practically the same along the entire length of the contact with the substrate.

Metallic coatings on a silicon–carbon film were obtained by vacuum magnetron sputtering. The thickness of the obtained coatings is Al—115 nm, Cr—90 nm, In—85 nm, Mo—70 nm, and W—35 nm. The interface between the applied metallic coatings of Al, Cr, In, Mo, and W and the silicon–carbon substrate is traced throughout the entire survey area. All samples of metallic coatings (Al, Cr, In, Mo, and W) have a microstructure close to the columnar one.

The tungsten coating has the worst adhesion strength with the silicon–carbon film ($L_{c3} = 4.86$ N, while the chromium coating has the best adhesion strength ($L_{c3} = 6.51$ N). The first scratches appear most quickly on the chromium coating ($L_{c1} = 1.47$ N), and the molybdenum coating remains without cracks the longest ($L_{c1} = 2.98$ N).

Further research should be directed to studying the adhesion strength of a wider range of metallic coatings with silicon–carbon films, as well as finding ways to improve the adhesion strength.

Author Contributions: Data curation, D.S.R.; Formal analysis, V.I.P.; Funding acquisition, V.I.P.; Investigation, S.V.Z., R.V.S. and D.S.R.; Methodology, N.I.C.; Validation, S.N.D.; Visualization, S.N.D.; Writing—original draft, N.I.C.; Writing—review and editing, A.I.G. All authors have read and agreed to the published version of the manuscript.

Funding: This work was realized using the equipment of the High Technology Center at BSTU named after V.G. Shukhov, the framework of the State Assignment of the Ministry of Education and Science of the Russian Federation, project No. FZWN-2023-0004.

Institutional Review Board Statement: Not applicable.

Informed Consent Statement: Not applicable.

Data Availability Statement: Not applicable.

Conflicts of Interest: The authors declare no conflict of interest.

References

1. Zare, E.N.; Iftekhar, S.; Park, Y.; Joseph, J.; Srivastava, V.; Khan, M.A.; Makvandi, P.; Sillanpaa, M.; Varma, R.S. An overview on non-spherical semiconductors for heterogeneous photocatalytic degradation of organic water contaminants. *Chemosphere* **2021**, *280*, 130907. [[CrossRef](#)] [[PubMed](#)]
2. Saraswat, S.; Tomar, V.K.; Deolia, V.K.; Mehta, N. A brief review of amorphous semiconductors. *Mat. Today Proc.* **2023**. [[CrossRef](#)]
3. Guarino, R.; Lewandowska, M.; Dembkowska, A.; Bykovskiy, N.; Sarasola, X.; Sedlak, K. Thermal-hydraulic analysis of alternative cable-in-conduit conductors for the European DEMO hybrid central solenoid. *Fusion Eng. Des.* **2023**, *187*, 113368. [[CrossRef](#)]
4. Kabanova, N.A.; Morkhova, Y.A.; Antonyuk, A.V.; Frolov, E.I. Prospective oxygen-ion conductors $\text{Ln}_a\text{X}_b\text{O}_z$: Geometry and energy calculations. *Solid State Ion.* **2023**, *391*, 116142. [[CrossRef](#)]
5. Pavlenko, V.I.; Cherkashina, N.I.; Demkina, L.N. Influence of Hydrothermal Treatment on Crystalline Form of SiO_2 Synthesized by Sol-Gel Method. *IOP Conf. Ser. Mater. Sci. Eng.* **2018**, *327*, 052026. [[CrossRef](#)]
6. Pavlenko, V.I.; Cherkashina, N.I. Synthesis of hydrophobic filler for polymer composites. *Int. J. Eng. Technol.* **2018**, *7*, 493–495. [[CrossRef](#)]
7. Abreu, J.S.; Costa, L.M.; De Lazari Ferreira, L.; Gonçalves de Oliveira, R.K.F.; Costa de Souza, T.d.C.; Nunes, E.H.M.; Houmard, M. Hydrothermal treatment as a tool to tailor the mesoporous structure of sol-gel silica. *J. Non-Cryst. Solids* **2023**, *610*, 122323. [[CrossRef](#)]
8. Sun, R.; Zhou, J.; Wang, W. A boric acid-assisted hydrothermal process for preparation of mesoporous silica nanoparticles with ultra-large mesopores and tunable particle sizes. *Ceram. Int.* **2023**, *49*, 20518–20527. [[CrossRef](#)]
9. Gawęda, M.; Jeleń, P.; Bik, M.; Szumera, M.; Olejniczak, Z.; Sitarz, M. Spectroscopic studies on phosphate-modified silicon oxycarbide-based amorphous materials. *Spectrochim. Acta Part A Mol. Biomol. Spectrosc.* **2023**, *291*, 122341. [[CrossRef](#)]
10. Niemiec, W.; Szczygieł, P.; Olejniczak, Z.; Handke, M. The influence of carbon atom distribution in precursors with 1:1 carbon to silicon atoms ratio on structure and thermal evolution of obtained silicon oxycarbide based materials. *Ceram. Int.* **2021**, *47*, 33070–33077. [[CrossRef](#)]
11. Wang, S.E.; Kim, M.J.; Park, J.-S.; Lee, J.W.; Yoon, D.W.; Kim, Y.; Kim, J.H.; Kang, Y.C.; Jung, D.S. Silicon oxycarbide-derived hierarchical porous carbon nanoparticles with tunable pore structure for lithium-sulfur batteries. *Chem. Eng. J.* **2023**, *465*, 143035. [[CrossRef](#)]
12. Leonel, G.J.; Guo, X.; Singh, G.; Navrotsky, A. Compositional Analysis of SiOC(H) Powders: A Comparison of X-ray Photoelectron Spectroscopy (XPS) and Combustion Analysis. *Ceramics* **2023**, *6*, 74–85. [[CrossRef](#)]
13. Strachota, A.; Černý, M.; Glogar, P.; Sucharda, Z.; Havelcová, M.; Chlup, Z.; Dlouhy, I.; Kozák, V. Preparation of Silicon Oxycarbide Composites Toughened by Inorganic Fibers via Pyrolysis of Precursor Siloxane Composites. *Acta Phys. Pol. A* **2011**, *120*, 326–330. [[CrossRef](#)]
14. Zheng, S.; Sun, Q.Q.; Yang, W. Modulation in current density of metal/n-SiC contact by inserting Al_2O_3 interfacial layer. *Nanoscale Res. Lett.* **2013**, *8*, 116. [[CrossRef](#)]
15. Roccaforte, F.; Vivona, M.; Greco, G.; Lo Nigro, R.; Giannazzo, F.; Rascunà, S.; Saggio, M. Metal/Semiconductor Contacts to Silicon Carbide: Physics and Technology. *Mater. Sci. Forum* **2018**, *924*, 339–344. [[CrossRef](#)]
16. Averyanov, D.V.; Sokolov, I.S.; Parfenov, O.E.; Taldenkov, A.N.; Kondratev, O.A.; Tokmachev, A.M.; Storchak, V.G. A class of high-mobility layered nanomaterials by design. *J. Mater. Sci. Technol.* **2023**, *164*, 179–187. [[CrossRef](#)]
17. Mao, M.; Ke, S.; Tang, D.; Sang, X.; He, D. Structure and Performance Optimization of Co Magnetic Thin Films Deposited by Vacuum Evaporation Coating. *Materials* **2023**, *16*, 3395. [[CrossRef](#)] [[PubMed](#)]
18. Zaitsev, S.V.; Cherkashina, N.I.; Pavlenko, V.I.; Prochorenkov, D.S. Formation and stability of W coating on a flexible polyimide substrate. *Thin Solid Film.* **2020**, *715*, 138424. [[CrossRef](#)]
19. Wei, S.; Zheng, Q.; Wang, L.; Peng, C.; Cui, X.; Che, X.; Wang, W.; Yu, Z. Fabrication and Characterization of Mineral Hydrophilic Antifogging Film via Vacuum Evaporation Method. *Coatings* **2023**, *13*, 730. [[CrossRef](#)]

20. Liu, L.; Li, W.; Li, Z.; He, F.; Lv, H. Metal-Free Catalytic Preparation of Graphene Films on a Silicon Surface Using CO as a Carbon Source in Chemical Vapor Deposition. *Coatings* **2023**, *13*, 1052. [[CrossRef](#)]
21. Yao, K.-M.; Xu, M.; Huang, X.-Z.; Mo, D.-C.; Lyu, S.-S. Electrochemical deposition of copper films to develop the latent sebaceous fingerprints on metal substrates. *J. Electroanal. Chem.* **2023**, *941*, 117526. [[CrossRef](#)]
22. Ko, E.C.; Kim, J.Y.; Rhee, H.; Kim, K.M.; Han, J.H. Low-resistivity ruthenium metal thin films grown via atomic layer deposition using dicarbonyl-bis(5-methyl-2,4-hexanediketonato)ruthenium(II) and oxygen. *Mat. Sci. Semicond. Process.* **2023**, *156*, 107258. [[CrossRef](#)]
23. Popescu, A.-M.J.; Branzoi, F.; Burada, M.; Moreno, J.C.; Anastasescu, M.; Anasiei, I.; Olaru, M.T.; Constantin, V. CoCrFeMnNi High-Entropy Alloy Thin Films Electrodeposited on Aluminum Support. *Coatings* **2023**, *13*, 980. [[CrossRef](#)]
24. Gorlaeva, V.N.; Bisengaliev, R.A. Electrodeposition of Metals on p-Si from Aqueous Electrolytes. *Semiconductors* **2021**, *55*, 384–386. [[CrossRef](#)]
25. Asgary, S.; Vaghri, E.; Daemi, M. Magnetron sputtering technique for analyzing the influence of RF sputtering power on microstructural surface morphology of aluminum thin films deposited on SiO₂/Si substrates. *Appl. Phys. A* **2021**, *127*, 752. [[CrossRef](#)]
26. Kawabata, R.; Matsuda, T.; Seo, R.; Hirose, A. Metallization-free silver sinter bonding to silicon via in situ decomposition of silver oxalate. *Mater. Lett.* **2021**, *300*, 130205. [[CrossRef](#)]
27. Barbosa, N.; Ridley, R.S.; Strate, C.H. Metal Adhesion to <100> Si Substrates with Varying Surface Conditions. *MRS Online Proc. Libr.* **2001**, *695*, 791. [[CrossRef](#)]
28. Colombo, P.; Mera, G.; Riedel, R.; Soraru, G.D. Polymer-Derived Ceramics: 40 Years of Research and Innovation in Advanced Ceramics. *J. Am. Ceram. Soc.* **2010**, *93*, 1805–1837. [[CrossRef](#)]
29. Blum, Y.D.; Schwartz, K.B.; Laine, R.M. Pre-ceramic polymer pyrolysis. *J. Mater. Sci.* **1989**, *24*, 1707–1718. [[CrossRef](#)]
30. Thornton, J.A. Structure-zone models of thin films. *Proc. Soc. Photo-Opt. Instrum. Eng.* **1987**, *821*, 95–105.
31. Bull, S.; Rickerby, D.; Matthews, A.; Pace, A.; Leyland, A. Scratch Adhesion Testing of Hard, Wear Resistant Coatings. In *Plasma Surface Engineering*; Broszeit, E., Munz, W.D., Oechsner, H., Rie, K.-T., Wolf, G.K., Eds.; DGM Informationsgesellschaft Verlag: Oberursel, Germany, 1989; Volume 2, pp. 1227–1235.
32. Siddiqui, S.A.; Favaro, G.; Berkes Maros, M. Investigation of the Damage Mechanism of CrN and Diamond-Like Carbon Coatings on Precipitation-Hardened and Duplex-Treated X₄₂Cr₁₃/W Tool Steel by 3D Scratch Testing. *J. Mater. Eng. Perform.* **2022**, *31*, 7830–7842. [[CrossRef](#)]

Disclaimer/Publisher’s Note: The statements, opinions and data contained in all publications are solely those of the individual author(s) and contributor(s) and not of MDPI and/or the editor(s). MDPI and/or the editor(s) disclaim responsibility for any injury to people or property resulting from any ideas, methods, instructions or products referred to in the content.